26

G40-800/5260 Carbon Fiber/Bismaleimide Composite Material: High Temperature Characteristics of Static and Fatigue Strengths

Toshiyuki Shimokawa[1], Yoshiaki Kakuta[2] and Takenori Aiyama[3]
[1]*Formerly Tokyo Metropolitan Institute of Technology,*
[2]*Japan Aerospace Exploration Agency,*
[3]*Toyota Motor Corporation*
Japan

1. Introduction

A lot of polymer composite materials are being used in the structures of civil transport aircraft currently under development, such as the Boeing 787, Airbus A350, and Bombardier C Series. Their percentages of structural weight are announced at 50%, 53% and 46%, respectively. However, mostly carbon fiber/epoxy (CF/Ep) systems are being introduced into their primary structures and they are only being introduced in environments where they are not expected to encounter high temperature. On the other hand, application of carbon fiber/bismaleimide (CF/BMI) composite materials is being expanded, especially for military aircraft structures such as the airframes of the F-22 Raptor and the F-35 Lightning II Joint Strike Fighter, the jet engine nacelle skins of the F-35 as well as the thrust reverser structure of the Gulfstream G450 business jet in civil aircraft (McConnell, 2009), and is expected for structures of the next-generation supersonic transport (SST).

There are several reasons for CF/BMI system application for the structures described above. As for epoxy system composite materials, about 70°C is usually set as the design limit temperature for long term use (Brandecker & Hilgert, 1988, Fawcett et al., 1997). Meanwhile, carbon fiber/polyimide (CF/PI) system composite materials can be used for hotter structures, although they are very expensive and involve complicated processes. CF/BMI composite materials offer temperature performance and costs between those of epoxy and polyimide systems. Moreover, CF/BMI systems can be easy handled in an airframe parts manufacturing process in a way that is equivalent to that for epoxy systems.

The design limit temperature of CF/BMI composite materials for aircraft structures is supposed to be around 120°C on the basis of actual application to the mechanically loaded structures described above. If the design limit temperature is set as 120°C, it is necessary to know the detailed characteristics of static and fatigue strengths at about 150°C from the view point of the safety margin; moreover, 150°C is considered to be close to the service-limit temperature for CF/BMI composite materials. Therefore, in order to apply CF/BMI composite materials for aircraft structures that encounter medium high temperatures,

knowledge of their static and fatigue properties at 150°C is very important in comparison with that at RT.

The following reports presented the static strength of a CF/BMI composite material, G40-800/5260, with a quasi-isotropic layup. As part of the investigation of the potential of high temperature composite materials for the next-generation SST, the authors' group assessed open-hole (OH) tensile and compressive static strengths at RT and 120°C (Shimokawa et al., 1999-a). Hirano reported OH tensile and compressive static strengths at RT only (Hirano, 2001). Johnston and Gates investigated OH tensile static strength at from 23°C to 218°C (Johnston and Gates, 1998).

Meanwhile, the following investigations were carried out on fatigue strength or *S-N* relationships of CF/BMI composite materials with a quasi-isotropic stacking sequence at RT. Hirano conducted axial tension, compression, and tension-compression fatigue tests for OH specimens of a G40-800/5260 CF/BMI laminate along with CF/PI composite materials based on a small number of specimens and presented a rough estimate of *S-N* relationships (Hirano, 2001). For materials with a non quasi-isotropic stacking sequence, Gathercole et al. fatigue tested unnotched specimens of a T800/5245 CF/BMI laminate with $[(\pm 45, 0_2)_2]_S$ layup under constant amplitude loading over a wide range of stress ratio R (=minimum stress/maximum stress), and discussed Weibull life-distributions, *S-N* relationships, and Goodman's diagram based on an analysis of test results (Gathercole et al., 1994). Following this paper, Adam et al. reported the results of programmed fatigue tests of block variable loading, provided the cumulative damage fraction to failure, and discussed the applicability of a nonlinear cumulative damage rule (Adam et al., 1994). On the other hand, Tyahla and McClellan reported various kinds of test results on the durability and damage tolerance of IM6/3100 and IM6/F650 CF/BMI composite materials, including results of fatigue testing of OH specimens (Tyahla and McClellan, 1988). The layup of OH specimens was [0°(50%)/±45°(40%)/90°(10%)] and fatigue tests were carried out at only two or three stress levels for R=-1 and 10 under cold temperature dry (CTD), room temperature dry (RTD), and elevated temperature wet (ETW) conditions.

Although as described above many reports about the static and fatigue strengths of CF/BMI composite materials have been published, this chapter discusses only test results obtained for specimens with a quasi-isotropic layup, because such test results can be used for the reference or comparison data. Moreover, this chapter focuses on the high-temperature characteristics of the static and fatigue strengths.

For OH static strength at high temperatures, only data at 120°C by the authors and those of OH tensile strength by Johnston and Gates were reported. As for fatigue strength, Hirano only discussed rough *S-N* relationships of fatigue characteristics at RT as determined by axial tension, compression and tension-compression fatigue tests using a small number of test specimens. Under these circumstances, the authors systematically conducted static tests on NH and OH specimens and fatigue tests on OH specimens for a CF/BMI composite material with a quasi-isotropic layup at RT and high temperatures and discussed test results and the high-temperature practicality of this material (Shimokawa et al., 2008).

In this chapter the authors introduce the major contents of their previous paper from a practical viewpoint. The material used was a G40-800/5260 CF/BMI composite material selected from popular CF/BMI composite materials. The objective of this study was to systematically clarify static and fatigue strength at RT and 150°C. In addition, solely static compressive tests on NH specimens were conducted at several high temperatures up to

215°C. Static tests provided static tensile and compressive strengths of NH and OH specimens. Fatigue tests under constant amplitude loading provided *S-N* relationships for just the OH specimens, i.e., tension, compression, and tension-compression fatigue tests. Visual and CCD microscope observation showed the fracture behavior of static and fatigue failure.

The major subjects of this chapter are as follows. (1) An offer of reference data with respect to the static and fatigue strengths at RT and high temperatures. (2) Fiber dominant and matrix (resin) dominant properties in static and fatigue strengths. (3) Open-hole and temperature dependence on static strength. (4) The dependence of the stress ratio *R* (*R*=minimum stress/maximum stress in fatigue loading) and temperature on fatigue strength and *S-N* relationships. (5) The strength ratio (=compression strength/tension strength) for static and fatigue strengths. (6) The influence of load components on fatigue strength degradation, i.e., the influence of tension, compression, and tension-compression load cycles. (7) Practicality evaluation of static and fatigue strengths in the marginal high temperature region for long-term use.

2. Material, specimens and testing procedures

The prepreg system used is a combination of G40-800 CF and 5260 toughened BMI resin made by CYTEC Co. The lamination has a quasi-isotropic (QI) stacking sequence, 32 plies $[45/0/-45/90]_{4S}$. The nominal thickness of 4.29 mm (0.134 mm × 32) was used in calculating stress on specimens. Laminate panels were cured in an autoclave at 190°C for two hours at a pressure of 6.0 kgf/cm² and post-cured at 215°C for four hours in an air-circulating oven. All panels were cured at the same time.

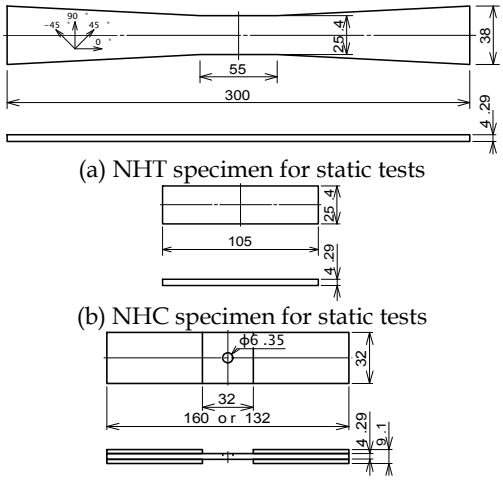

(a) NHT specimen for static tests

(b) NHC specimen for static tests

(c) Common specimen for OHT and OHC static and fatigue tests

Fig. 1. Specimen configurations for static and fatigue tests (mm)

Fig. 1 (a) and (b) illustrate specimen configurations for NH tensile and compressive static tests. Fig. 1 (c) shows the configuration of OH specimens used for both static and fatigue tests. To avoid the complex stress state of coupon-type fatigue leading to failure in the vicinity of the clamping location, only OH specimens were used for fatigue tests. The

clamping parts of OH specimens were bonded with tubs made of the same material as the specimens. In the static tensile and tension fatigue tests, a longer clamp was used, while the static compressive tests, and compression fatigue and tension-compression fatigue tests used the shorter grip size shown in Fig. 1 (c). Laminate processing and specimen manufacturing were carried out at Kawasaki Heavy Industries, Ltd.

For generality, specimen configurations conform to ASTM standards or SACMA recommendations. Since the objectives of this study included the direct comparison of NH static and OH static strengths, the use of common OH specimens for comparing OH static and fatigue strengths, and specimen cost reduction, the specimen configuration shown in Fig. 1 (c) was employed. In particular, the cross-sectional area was equal for both NH and OH specimens. The hole diameter of OH specimens in this study was that from SACMA recommended methods, and other dimensions were smaller than those in the SACMA methods. Table 1 shows the number of specimens tested, with the number of run-out specimens for which the fatigue test was suspended given in parentheses.

Temperature (°C)	Static test specimen				Fatigue test, OH specimen		
	NHT	NHC	OHT	OHC	R=0.1	R=10	R=-1
RT	4	3	2	4	10(2)	8	7
120	–	1	–	–	–	–	–
150	3	3	2	4	5	7	5
180, 215	–	1 each	–	–	–	–	–

Number in ( ) represents run-out specimens

Table 1. Number of specimens used for static and fatigue tests

An INSTRON 8500 digitally-controlled servo-hydraulic material testing machine with an environmental chamber was used for static and fatigue tests. Static tensile tests for NH and OH specimens and static compressive tests for OH specimens were conducted using hydraulic grips. Static compressive tests for NH specimens were conducted using the NAL (National Aerospace Laboratory) type compression test fixture (Shimokawa et al., 1999-a, 1999-b, 2002) shown in Fig. 2. A supporting guide for both clamps seen in Fig. 2(a), which has a fine clearance to the top clamp, prevents moving of the clamps in the out of plane direction of the specimen. The test part of the specimen is not supported against out of plane bending. The compression load is given from both end-sections of the specimen. The actuator speed of the testing machine for all static tests was 1 mm/min.

Fatigue tests were conducted under sinusoidal constant amplitude loading with a repetition frequency of 1 Hz or 5 Hz. Three kinds of stress ratio, R=minimum stress/maximum stress, were selected, i.e., R=0.1 for tension fatigue tests, R=10 for compression fatigue tests, and R=-1 for tension-compression fatigue tests.

The temperature in the laboratory was controlled by an air conditioner at around 23°C throughout the year. Static and fatigue tests at high temperatures used an air-circulating environmental chamber (Shimokawa et al., 2007). Elevated temperature tests were mainly conducted at 150°C, as indicated in Table 1. For the static NH compressive tests only, several temperatures were chosen up to 215°C in order to estimate the effect of the heat-resistance of the BMI resin with respect to compressive strength. Stress in OH specimens in this study is represented by the net section stress,

$$S = \frac{P}{(W-d)t} \tag{1}$$

where P is applied load, W specimen width, d open hole diameter, and t the nominal thickness of a specimen. Failed specimens were inspected visually and with a CCD microscope to determine the failure mode: fiber dominant or matrix dominant.

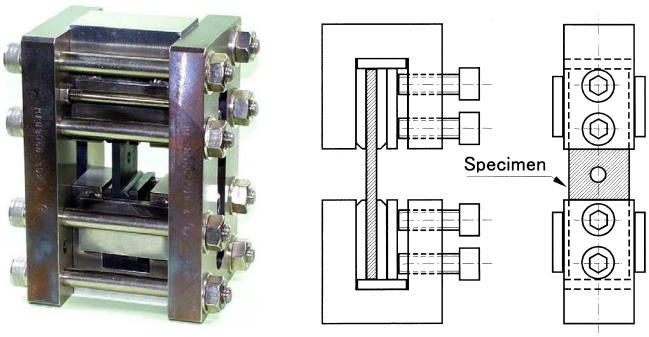

(a) Overview (b) Clamping assembly

Fig. 2. NAL type compression test fixture

3. Test results

Table 2 presents the numerical data of static strength S_u and its mean $\overline{S}_u$, while Table 3 presents fatigue life data. These data were systematically obtained as described above and are expected to be used for the reference or comparison data for conventional CF/BMI composite materials and new CF/BMI materials recently developed for low-cost and out-of-autoclave manufacturing such as those produced by a VaRTM (Vacuum assisted Resin Transfer Molding) method.

Specimen	Load	Temp. (°C)	Strength S_u (MPa)	Mean $\overline{S}_u$ (MPa)
NH	Tens.	RT (23)	1016, 1060, 1116, 1126	1079
		150	871, 1000, 1033	968
	Comp.	RT (23)	834, 884, 899	872
		120	751	751
		150	651, 652, 659	654
		180	586	586
		215	246	246
OH	Tens.	RT (23)	704, 724	714
		150	672, 708	690
	Comp.	RT (23)	409, 446, 476, 514	461
		150	376, 377, 391, 408	388

Table 2. Static strength data

Fat. Load (R)	T (°C)	S-N relationship: S=S_{max} or S_{min} (MPa), N=Number of cycles to failure								
Tens. (0.1)	RT (23)	S	688	688	652	652	651	616	614	580
		N	5	134	553	8,960	338,223	211,916	*89,000	4,313,329
	150	S	674	639	638	602	567		580	579
		N	8	62,283	3,469	67,000	445,500		*1,000,000	5,760,765
Comp. (10)	RT (23)	S	-410	-387	-387	-364	-364	-364	-319	-318
		N	3,150	7,771	8,891	16,294	38,871	47,191	836,882	2,112,567
	150	S	-356	-356	-336	-336	-316	-316	-277	
		N	807	1,734	2,428	13,558	225,944	261,779	6,726,000	
Tens.-Comp. (-1.0)	RT (23)	S	387	387	364	341	319	318	273	
		N	460	5,583	11,197	24,210	81,004	76,457	851,768	
	150	S	336	316	277	277	240			
		N	892	15,114	132,437	239,397	1,182,763			

R=stress ratio, T=temperature, * indicates no failure

Table 3. Fatigue life data

3.1 Static strength of NH and OH specimens

Fig. 3 shows non-hole tensile (NHT) strength, non-hole compressive (NHC) strength, open-hole tensile (OHT) strength, and open-hole compressive (OHC) strength at RT and high temperatures, where OH strength is represented by net section stress, as described above. Since these tests were carried out to determine their temperature dependence, only a few specimens were tested for each case, as shown in Table 1. The relationship between static strength and temperature is represented by a solid line, which connects the mean strength at every test temperature. When there is only one test result, this value is taken as the mean.

NHT strength at 150°C is slightly lower than that at RT. Although this fact is strongly influenced by the lowest value measured at 150°C (Fig. 3), this tendency is considered to be reasonable if referred to the tendency that appeared in OHT static strength (Fig. 3) and OHT fatigue strength, as described later. When the mean values are compared, the NHT strength at 150°C is 10% lower than that at RT. Since the usual allowable temperature limit of carbon fibers is about 538°C (1000°F) (Niu, 1996), the strength of carbon fibers in the material tested is considered unchanged between RT and 150°C. Furthermore, since all 0° fibers needs to be broken for the final failure of the material tested, the tensile strength is dominated by the fiber strength, i.e., it is considered to be a fiber-dominant property. However, the small decrease in tensile strength found at 150°C means that the matrix binding the fibers also has a small effect on tensile strength, so this is not entirely a fiber-dominant property. This aspect will be discussed in detail later on the basis of careful examination of failed specimens. On the other hand, the mean OHT strength at 150°C is only 3% lower than that at RT. Although this reduction is quite small in comparison with that of NHT strength, this tendency to decrease with increasing temperature is common for NHT and OHT strengths.

NHC strength decreases considerably with increasing temperature and the mean NHC strength at 150°C is 25% lower than that at RT. Furthermore, although NHC strength drops gently up to 180°C, it drops heavily at 215°C. The compressive strength of both NH and OH specimens is considered to be a matrix-dominated property. Although this study did not measure the glass transition temperature of the material tested, Johnston and Gates reported

that the glass transition temperature of a G40-800/5260 CF/BMI composite was about 228°C after the material was left in a laboratory environment for several days (Johnston and Gates, 1998). Therefore, this heavy drop of the compressive strength of NH specimens is understandable. The decrease in NHC strength with temperature rise is considered to be a reflection of the decrease in matrix strength in that the specimen failure mechanism is not changed. The mean OHC strength at 150°C is 16% lower than that at RT and this drop is not very large, though it is larger than that of the mean OHT strength. The above results indicate that high temperatures have a large effect on NHC strength, but have a comparatively small effect on other strengths, i.e. NHT, OHT, and OHC strengths. The favorable test results mentioned above are considered to have appeared due to the effectiveness of using heat-resistant polymer as the matrix.

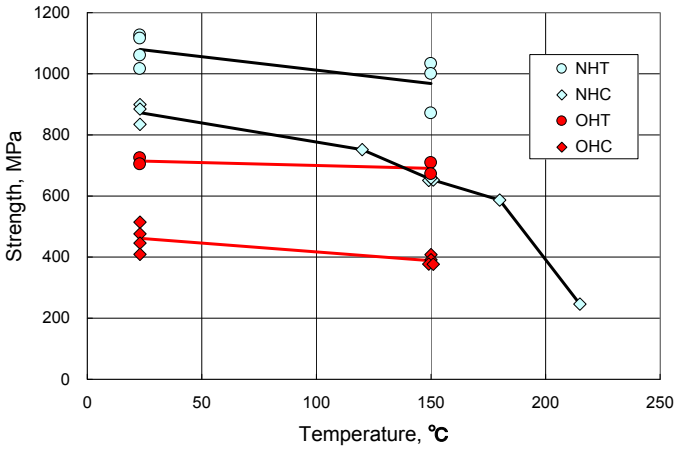

Fig. 3. Static tensile and compressive strengths of NH and OH specimens as a function of temperature

3.2 Fatigue strength of OH specimens

Let us examine *S-N* (stress-life) relationships on semi-logarithmic graph paper based on net section stress, placing the maximum stress S_{max} on the ordinate and the logarithm of fatigue life log*N* on the abscissa, where *N* is the number of load cycles to failure. In compression fatigue, the minimum stress S_{min} is used instead of S_{max} on the ordinate. If *N* is assumed to be an independent variable on the *S-N* diagram, S_{max} will be a dependent variable and can be regarded as fatigue strength. OH static strength is plotted as S_{max} at N=1 to compare it with fatigue strength. An *S-N* relationship is assumed to be linear on semi-logarithmic graph paper. The *S-N* line approximating only *S-N* data is determined by the least-squares method.
The *S-N* equation is represented by

$$S_{max} = a - b \cdot \log N \tag{2}$$

where *a* and *b* are constants and treated as parameters, i.e., intersection and slope. Since the slope of the *S-N* relationship in this study is quite small, *N* is dealt with as an independent variable and S_{max} as a dependent variable to aid intuitive understanding. Table 4 shows the

parameters of *S-N* equations for three kinds of *R*. In order to discuss tension-compression fatigue-test results later, the S_{range}-*N* relationship for compression fatigue is also shown in Table 4, where S_{range} (=S_{min}-S_{max}) is the compression repeated stress range.

Fatigue test & *S-N* relationship	Temp.	Parameters	
		a (MPa)	*b* (MPa)
Tension, S_{max}-*N*, (*R*=0.1)	RT	714	18.9
	150°C	698	18.9
Compression, S_{min}-*N*, (*R*=10)	RT	-510	-31.4
	150°C	-410	-18.6
Tension-compression, S_{max}-*N*, (*R*=-1)	RT	508	38.2
	150°C	433	30.4
Compression, S_{range}-*N*, (*R*=10)	RT	459	28.3
	150°C	369	16.7

Table 4. Parameters of *S-N* equations

3.2.1 Tension fatigue strength

Fig. 4 shows the static OHT strength and *S-N* relationships from tension fatigue tests for *R*=0.1 at RT and 150°C. In the RT fatigue tests, an arrow shows those run-out specimens whose fatigue tests were terminated without specimen failure; however, these points were included in the *S-N* data when approximated by an *S-N* line. Therefore, the *S-N* line at RT provides a conservative estimate. From the two *S-N* lines in this figure and the *b* values in Table 4, the *S-N* relationships at RT and 150°C have equal slopes and are considered to be parallel. Moreover, the difference between fatigue strength at RT and 150°C is close to the difference of the mean static strength at *N*=1 regardless of *N*. That is, the test results showed that the difference in static strength in the two environments appeared in the difference in fatigue strength. This fact points out that a difference between the *S-N* lines at RT and 150°C exists but it is very small. Furthermore, since the slope of the *S-N* line is small, the decrease in S_{max} is small with an increase in *N* at either RT or 150°C.

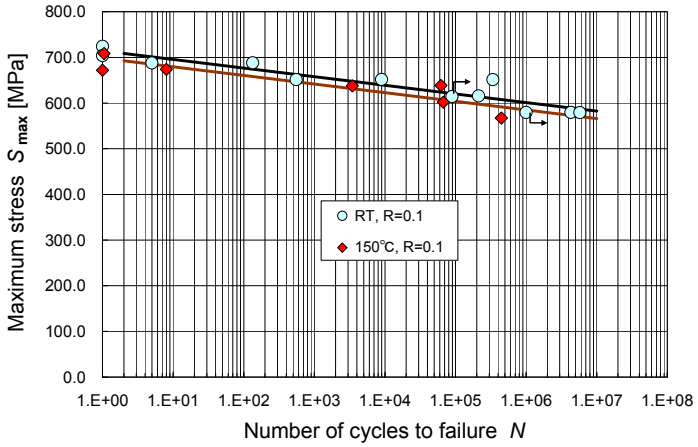

Fig. 4. *S-N* diagram of OH specimens from tension fatigue tests, *R*=0.1, at RT and 150°C

The mean tensile static strength is 714 MPa at RT and 690 MPa at 150°C in Table 2. Meanwhile, the intersection *a* in Table 4 is 714 MPa at RT and 698 MPa at 150°C. Although there is a slight difference between the static strength and the intersection of the *S-N* line at 150°C, static strength can be treated as a part of the *S-N* relationship for *R*=0.1 in both environments.
The fact that tension fatigue strength is slightly influenced by temperature and load repetition means that it is strongly fiber-dominated. However, since these small effects are real, the fiber dominance is not total.

3.2.2 Compression fatigue strength

Fig. 5 presents the static OHC strength and *S-N* relationships obtained from compression fatigue tests for *R*=10 at RT and 150°C. From the two *S-N* lines in this figure and the *b* or *b*/*a* values in Table 4, compression fatigue strength S_{min} at RT and 150°C drops considerably with the increase in the number of load cycles *N*. Moreover, there is a clear difference between the two *S-N* lines at RT and 150°C. However, as *N* becomes larger, the difference between the lines tends to decrease.
The values of intersection *a* in Table 4 are very close to the highest values of static compressive strength plotted at *N*=1 for the RT and 150°C conditions, and higher than their mean in Table 2. Since the scatter of static compressive strength at RT is fairly large, the difference between the highest and mean values is fairly large. The static compressive strength is judged not suitable for regarding as a part of the *S-N* relationship. In contrast, at 150°C the static compressive strength has a small scatter and may be regarded as a part of the *S-N* relationship. However, generally including the data on static compressive strength in the compression fatigue data cannot be recommended.
As mentioned above, since the compression fatigue strength is greatly influenced by temperature and the number of load cycles, it becomes apparent that compression fatigue strength is a matrix-dominated property.

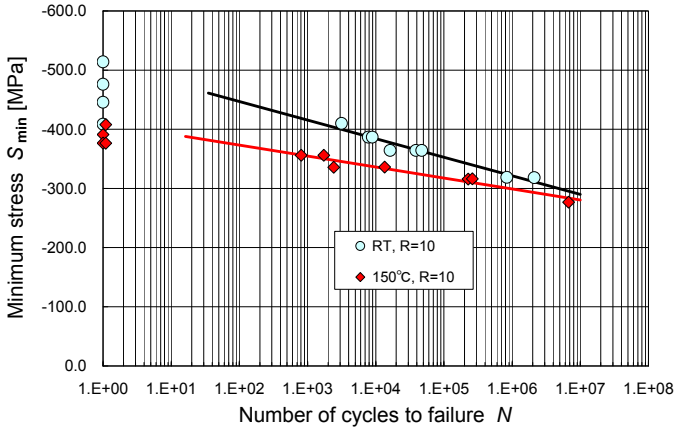

Fig. 5. *S-N* diagram of OH specimens from compression fatigue tests, *R*=10, at RT and 150°C

3.2.3 Tension-compression fatigue strength

Fig. 6 shows the static OHC strength and *S-N* relationship obtained from tension-compression fatigue tests for *R*=-1 at RT and 150°C. Since compression load repetition

greatly influences fatigue life in tension-compression fatigue tests, as described later, static OHC strength was plotted at N=1 as in the case of compression fatigue. According to the S-N lines at RT and 150°C and the b values in Table 4, S_{max} apparently decreases with increasing N. Moreover, there is an apparent difference between the two S-N relationships at RT and 150°C, as was the case in the compression fatigue tests. The tension-compression fatigue strength is strongly dependent on temperature and the number of load cycles, as in the compression fatigue tests.

Furthermore, these S-N lines pass fairly above their mean compressive strengths given by compressive $\overline{S}_u$ in Table 2. Generally, $\overline{S}_u$ is considered to be not included in the S-N lines in Fig. 6 at both RT and 150°C.

As mentioned above, since the tension-compression fatigue strength is strongly influenced by temperature and the number of load cycles, it is also judged to be a matrix-dominant property.

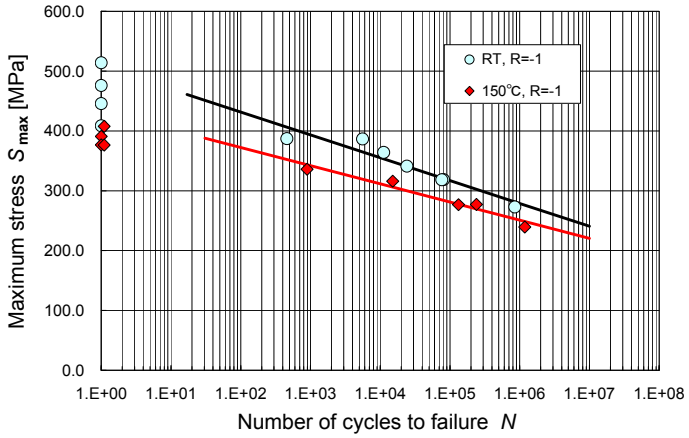

Fig. 6. S-N diagram of OH specimens from tension-compression fatigue tests, R=-1, at RT and 150°C

4. Detailed discussion of test results

4.1 Fiber-dominant strength, matrix-dominant strength, and failure modes

As described above, static tensile strength and tension fatigue strength are predominantly fiber-dominant, and static compressive strength and compression and tension-compression fatigue strengths are matrix-dominant. This section discusses the fiber-dominant and matrix-dominant characteristics of static and fatigue strengths based on observations of specimen failure and failure modes. The mechanical properties of carbon fibers are considered to be constant over the range from RT to 215°C. Moreover, since no signs of fatigue damage were found in the fibers themselves, any fatigue strength reduction of carbon fibers can be left out of consideration. Therefore, matrix damage influenced by temperature and load repetition is considered to generate the temperature dependence of the static and fatigue strengths, and also the load cycle dependence of fatigue strength.

Initially, we will consider static NHT strength. In order to generate tensile failure in an NH specimen, fibers in the 0° fiber layers that directly bridge both end regions where the load is

introduced must finally be broken. If static tensile strength is determined only by 0° fiber fracture, temperature dependence will not appear and perfect fiber dominance will be seen. However, both the static NHT and OHT strengths in Fig. 2 indicate small temperature dependence. This means that the matrix has a small effect on static tensile strength. This aspect can be clarified by examining the failure mode of a specimen. The load-displacement diagram observed in a static tensile test of an NH specimen was considered to be linear up to final failure. In addition, fibers in the 45° fiber layers did not bridge both ends where the load was introduced. Thus geometry tells us that if 45° fiber layers also share internal load via the matrix until the fracture of 0° fiber layers, the final strength of the laminate will become higher than if only 0° fiber layers share internal load. This phenomenon can be evaluated by inspecting whether fiber fracture exists in the 45° layers after final specimen failure.

Fig. 7 shows surface and side views of static tensile failure in NH and OH specimens. A surface view of static tensile fracture in an NH specimen at RT is shown in Fig. 7(a). The front line of the surface 45°-fiber-layer fracture intersects with the 45° fiber direction at 90°. In addition, the 45° fiber layer was also cut at the load-axis orientation. This is evidence that the ±45° fiber layers shared the axial load via the matrix until just before the final specimen fracture. Since the fiber binding strength of the matrix will decrease with increasing temperature, the load sharing rate of the ±45° fiber layers will decrease at the same time. Fig. 7(b) shows the static tensile fracture of an OH specimen at RT, with surface and side views from the same specimen. As shown in the left-hand figure, only a small number of surface +45° fibers failed. The right-hand figure displays small slits in a comb pattern produced by fiber separation in the -45° fiber layers in the upper part of the side face. Such slits extended even to the lower part of the opposite face. In the lower part of the slits in the right-hand figure, delaminations produced by the pull-out of 0° fibers can be seen. These facts mean that +45° fibers fractured inside the specimen. Static OHT strength dropped slightly with increasing temperature similarly to static NHT strength, as shown in Fig. 3. However, the matrix binding strength decreases at elevated temperatures in comparison with that at RT, and stress concentration around the open hole is considered to drop at elevated temperatures. Therefore, this is a possible reason why OHT strength has small temperature dependence but does not fall in the same way as NHT strength at 150°C.

Next, we consider static compressive failure. The compressive strength of a composite material is considered to reflect the temperature dependence of the matrix strength. Fig. 8 shows the appearance of static NHC failure, which formed a rhombus shape in the side view. The main failure mechanism is considered to be compressive buckling failure generated by delamination progressing from micro-buckling. Partial shear fracture in the side view is also confirmed. This macroscopic shear fracture can be considered to have progressed from kinking initiation. Since these mechanisms of compression failure initiation depend on matrix strength (Pilato & Michno, 1994), the compressive strength is directly related to the temperature-dependent matrix strength. Fig. 9(a) and (b) show side views of static compression failure of different OH specimens at 150°C. Around the cross section having an open hole, macroscopic rhombus-shaped failure and shear failure in the thickness direction can be seen. Figure 9(a) shows typical rhombus-shape failure and the fracture mode in Fig. 9(b) seems to be shear-dominant; however, the fracture mode around the hole has a rhombus shape. Though the compressive fracture mechanism in an OH specimen is similar to that in an NH specimen, the drop of compressive strength at 150°C from RT is smaller than that of an NH specimen. This phenomenon is considered to originate in the relaxation of stress concentration around the hole at 150°C.

In the case of tension fatigue, matrix damage such as transverse micro-cracking and small delamination occurs in the open-hole wall and grows with the increase in the number of load cycles, and the 0° fiber layers gradually charge themselves with the load that ±45° fiber layers shared. Specimen failure will occur when the 0° fiber layers are loaded up to the limit load or the limit strain to failure. This means that although fatigue strength is influenced by high temperature and load repetition, there is a compensating effect as high temperature and load repetition reduce stress concentration around the open hole. Therefore, the tension fatigue strength is strongly fiber-dominant; however, it is slightly influenced by high temperature and the number of load cycles.

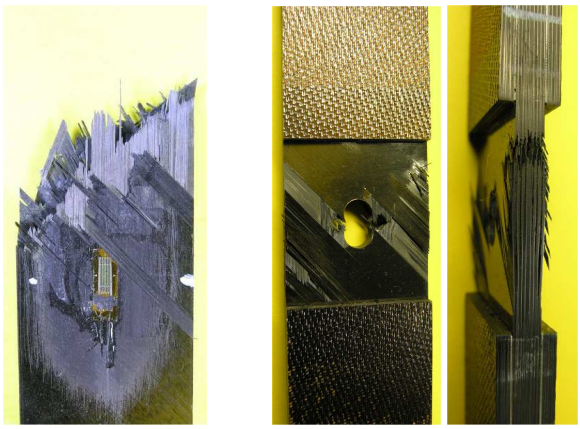

(a) NH specimen, RT (b) OH specimen, RT

Fig. 7. Surface and side views of static tensile failure of NH and OH specimens

Fig. 8. External view of static compressive failure of an NH specimen at RT

In the case of compression fatigue, fatigue damage such as transverse micro-cracking and small delamination occurs in the open-hole wall and delamination and local buckling progress, finally resulting in compression buckling failure. Inspection also showed partial shear fracture in the thickness direction. Thus, compression fatigue strength is governed by matrix failure and dependent on temperature and the number of load cycles. Additionally, the relaxation effect of stress concentration around the hole on compression fatigue strength is superimposed, producing the *S-N* relationships shown in Fig. 5. Rosenfeld and Gause also

pointed out that compression fatigue strength is matrix-dominated for a CF/epoxy composite material (Rosenfeld & Gause, 1981).

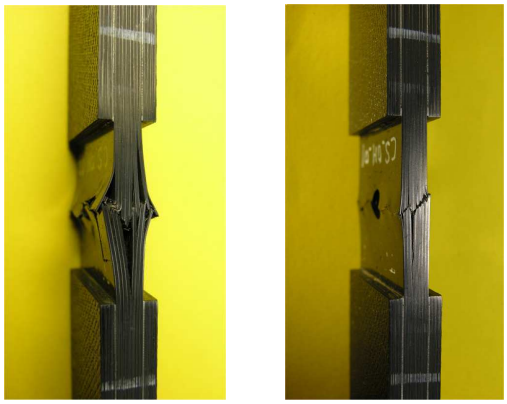

(a) OH specimen, 150°C (b) OH specimen, 150°C

Fig. 9. Side views of static compressive failure of OH specimens

In tension-compression fatigue, the final failure mode was similar to that of compression fatigue, i.e. delamination buckling. This fact suggests the important role of compression load repetition promoting delamination growth. The tension load component is also thought to contribute to delamination buckling by accelerating the initiation and growth of matrix damage. That is, the fatigue failure mode in tension-compression fatigue can be considered to be matrix-dominant and the tension-compression fatigue strength is dependent on temperature and the number of load cycles.

As mentioned above, since static compressive strength, compression fatigue strength, and tension-compression fatigue strength can be classified as matrix-dominant properties, the effectiveness of using a high-temperature resin as a matrix in an elevated temperature environment can be established. This viewpoint is very important and discussed again later.

4.2 Effect of an open hole on static strength and its temperature dependence

This section discusses the ratio of static OH strength to static NH strength and its temperature dependence, where this ratio is calculated from the mean strength based on the test results in Table2 or Fig. 3. Since the cross section of OH specimens was equal to that of NH specimens and the static strength was represented by the net section stress in this study, the experimental results are directly comparable.

Table 5 shows the ratios of the mean OH strength $\overline{S}_{UO}$ to the mean NH strength $\overline{S}_{UN}$, where $\overline{S}_{UO}$ is represented by the net section stress, calculated from the data at RT and 150°C.

$$r_{notch} = \frac{\overline{S}_{UO}}{\overline{S}_{UN}} \tag{3}$$

This table indicates that an open hole greatly reduces static strength for both tensile and compressive loading. The effect of stress concentration produced by the open hole is clearly apparent. Moreover, comparison of the reduction in tensile strength and compressive

strength shows that compressive strength decreases more than tensile strength does at either RT or 150°C. Furthermore, the strength reduction ratio due to the open hole at RT is larger than that at 150°C. This fact is explained by the relaxation of stress concentration around the open hole due to resin softening at 150°C, as described above.

Comparison	Temp.	r_{notch} (%)
Tensile strength ratio, OHT/NHT	RT	66
	150°C	71
Compressive strength ratio, OHC/NHC	RT	53
	150°C	59

Table 5. Effect of an open-hole on static strength represented by the ratio of the mean static strength of OH specimens to that of NH specimens

The following published data obtained at only RT were found. OHT/NHT strength ratios are 57% for T650-35/Radel 8320 CF/thermoplastic resin (Pilato & Michno, 1994), 58% for T800S/3900-2B and 56% for T800H/3900-2 CF/epoxy (JAXA, 2007). OHC/NHC strength ratios are 52% for T800H/F655-2 CF/BMI (Marais et al., 2001) and 51%-53% for T800S/3900-2B and T800H/3900-2 CF/epoxy (Nagao et al., 2007). Therefore, the numerical values presented in Table 3 are considered reasonable. The authors discussed the effect of an open hole on the static strength of CFRPs in detail based on theoretical formulae and test results (Shimokawa et al., 2008).

4.3 Comparison of RT and 150°C strengths subjected to static or fatigue loading

To examine the high-temperature performance of the material tested, we will discuss the ratio of 150°C strength to RT strength when the specimens are subjected to either static or fatigue loading. This strength ratio, $r_{150}(N)$, is defined as

$$r_{150}(N) \equiv \frac{150°C\ strength(N)}{RT\ strength(N)} \tag{4}$$

where static strength is given for N=1.

Table 6 indicates $r_{150}(N)$ values calculated by Eq. (4) for NH and OH specimens. Since the static strength ratio was described in Section 3.1, this section gives only numerical values in Table 6 for the sake of comparison. In the case of fatigue strength, the ratio was calculated by the *S-N* equation, Eq. (2), and the parameters in Table 4. For OH specimens the 150°C fatigue strength is adequately high in comparison with RT fatigue strength. In addition, the ratio of OHT fatigue strength agrees with that of OHT static strength. Furthermore, the ratio for OHC fatigue strength is larger than that for OHC static strength, i.e., the reduction in fatigue strength is smaller than that in static strength. This result is remarkable. Moreover, the tension-compression fatigue strength of OH specimens was adequately high at 150°C in comparison with that at RT.

As mentioned above, a high ratio listed in Table 6 for static and fatigue strengths indicates the high temperature performance of the material tested, and can be evaluated to demonstrate sufficient practical utility from the viewpoint of static and fatigue strength at 150°C.

Specimen and loading	Static strength ratio, $r_{150}(1)$	Fatigue strength ratio, $r_{150}(N)$			
		N=10⁴	N=10⁵	N=10⁶	N=10⁷
NH tension	90 %	-	-	-	-
NH compression	75 %	-	-	-	-
OH tension	97 %	97 %	97 %	97 %	97 %
OH compression	84 %	88 %	90 %	93 %	97 %
OH tension-compression	-	88 %	89 %	90 %	92 %

Table 6. The ratio of strength at 150°C to that at RT, $r_{150}(N)$, for NH and OH specimens given by the mean static strength and the fatigue strength calculated from the $S_{\max}$-N equation

4.4 Ratio of compression strength to tension strength in static and fatigue strengths

We now discuss the ratio of static compressive strength to static tensile strength in NH and OH specimens, and the ratio of compression fatigue strength (R=10) to tension fatigue strength (R=0.1) in OH specimens. That is, this section evaluates the weakness of the material tested for compression loading on the basis of the ratio of compression strength to tension strength.

The fatigue strength ratio for arbitrary N is defined by

$$r_{CT}(N) = -\frac{S_{comp,\min}(N)}{S_{tens,\max}(N)} \tag{5}$$

where $S_{comp,\min}(N)$ is compression fatigue strength (R=10), and $S_{tens,\max}(N)$ tension fatigue strength (R=0.1). The static strength ratio is defined for N=1, $r_{CT}(1)$, where $S_{comp,\min}(1)$ is the mean compressive strength and $S_{tens,\max}(1)$ the mean tensile strength. Fatigue strength is calculated by Eq. (2) and the parameters given in Table 4.

Table 7 indicates the calculated strength ratio, $r_{CT}(N)$. The static strength ratio of NH specimens is 81% at RT and 68% at 150°C. As described below, this ratio at RT is considered reasonable; however, it is fairly small at 150°C. This tendency is reflected in the compressive strength reduction presented in Fig. 3. On the other hand, the static strength ratio of OH specimens is 65% at RT and 56% at 150°C. That is, an open hole reduces this ratio further.

Moreover, the following published examples obtained at RT were found for the static strength ratio. For NH specimens of CF/epoxy composites, the static NHC/NHT strength ratio was 77% (JAXA, 2007) and 84% (Nagao et al., 2007) for two cases of T800S/3900-2B, and 83% for T800H/3900-2 (JAXA, 2007). For OH specimens, the static OHC/OHT strength ratio was 57% and 66% for T800S/3900-2B and T800H/3900-2 CF/epoxy composites, respectively (JAXA, 2007), and 67% (Shimokawa et al., 1999-a) and 68% (Hirano, 2001) for G40-800/5260 CF/BMI composites. Therefore, the numerical values of the static strength ratio in Table 7 are considered reasonable as compared with other test results.

As shown in Table 7, the fatigue OHC/OHT strength ratio is in the range of 50% to 60% at RT and 150°C. It is lower than that of static strength and has a tendency to decrease with the increase in the number of load cycles. Moreover, there is a tendency for the ratio at 150°C to be slightly lower than that at RT. Since compression strength is expected to be lower than

tension strength because of being a matrix-dominant property, these quantitative values are very important from an engineering perspective. This property should be fully taken into account in the design of composite structures.

Comparison	Temp.	Static strength ratio	Fatigue strength ratio			
			N=10^4	N=10^5	N=10^6	N=10^7
NHC/NHT	RT	81 %	-	-	-	-
	150°C	68 %	-	-	-	-
OHC/OHT	RT	65 %	60 %	57 %	53 %	50 %
	150°C	56 %	54 %	53 %	51 %	50 %

Table 7. The ratio of compression strength to tension strength, $r_{CT}(N)$, for NH and OH specimens: static strength ratio=mean compressive strength/mean tensile strength, and fatigue strength ratio=compression fatigue strength (R=10)/tension fatigue strength (R=0.1)

4.5 Effect of compression load cycles on tension-compression fatigue strength

The repeated stress range, $S_{range,}$ of compression fatigue tests (R=10) in this study is calculated by S_{range}=-0.9×S_{min}. If the S_{range}-N relationships in Fig. 5 are noticed, it can be understood intuitively that they are very close to the tension-compression S_{max}-N relationships in Fig. 6. These relationships are discussed in detail below.

S_{max} in tension-compression fatigue tests (R=-1) is the stress amplitude and indicates the tension stress range or compression stress range. Fig. 10 shows Fig. 6 itself together with the S_{range}-N relationships converted from the compression S_{min}-N relationships in Fig. 5. Thick lines are the tension-compression S_{max}-N relationships and fine lines represent the compression S_{range}-N relationships, whose parameters are given in Table 4. Fig. 10 indicates that two S-N relationships at RT broadly overlap over a wide range. When the parameters of two S-N lines at RT in Table 2 are compared, the S_{range}-N line of compression fatigue has a lower intersection and a lower slope than those of the tension-compression S_{max}-N line, respectively. It turns out that the two S-N lines at RT gradually intersect. Moreover, Fig. 10 means that compression load cycles contribute primarily to tension-compression fatigue strength and most tension-load cycles have little influence on tension-compression fatigue strength in the range for which fatigue data exists.

Two S-N lines at 150°C in Fig. 10 clearly intersect. However, the slopes of the two straight lines are not very different. Therefore, it is obvious that the repeated application of a compression load mainly affects tension-compression fatigue strength. In addition, the compression fatigue strength expressed by S_{range} is lower than the tension-compression fatigue strength in the life region shorter than where the two lines intersect. This tendency is explained as follows. With regard to the mean stress in a compression fatigue test (R=10), the mean stress and stress amplitude constitute the maximum compression stress, which generates the final fatigue failure due to delamination buckling. Next, since the tension-compression fatigue strength is equal to the compression fatigue strength expressed by S_{range} in the vicinity of the intersection, this means that the tension-load repetition in tension-compression fatigue tests did not affect the tension-compression fatigue strength, as in the case of the tension-compression S_{max}-N relationship at RT. Simultaneously, the mean compression stress in the compression fatigue test becomes smaller, and this is considered to not have any influence on fatigue strength. In the life range larger than the intersection, the

tension-compression fatigue strength becomes smaller than the compression fatigue strength expressed by S_{range} in Fig. 10, and this means that the tension-load repetition in a tension-compression fatigue test has an effect on delamination growth. The concept described above provides a coherent explanation for the *S-N* relationship at 150°C. Moreover, this kind of concept is also qualitatively applicable to *S-N* relationships at RT.

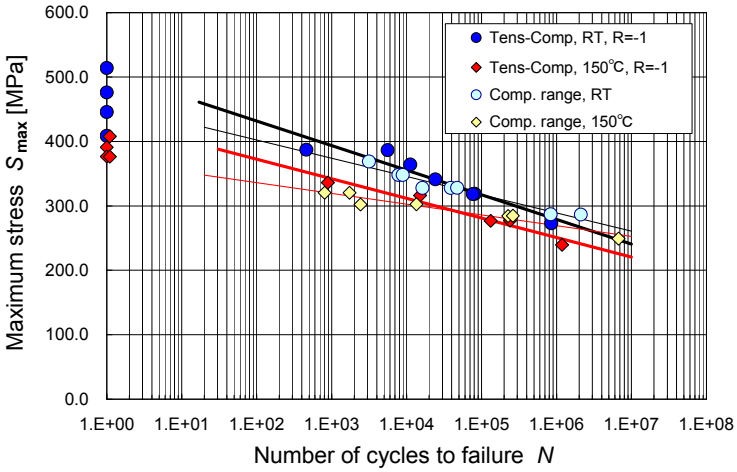

Fig. 10. *S-N* relationships from tension-compression fatigue tests and those showing the compression stress range from compression fatigue test results

The authors derived an S_{range}-*N* relationship from the compression S_{min}-*N* data (*R*=10) of NH specimens of a T800/5250 CF/BMI laminate with $[(\pm 45, 0_2)_2]_S$ layup given by Gathercole et al. (Gathercole et al., 1994) and compared it with the tension-compression S_{max}-*N* data (*R*=-1). This comparison showed that the S_{range}-*N* relationship (*R*=-1) was very close to the S_{max}-*N* relationship (*R*=-1) and the two *S-N* lines gradually intersected in almost the same manner as those at RT in Fig. 10. On the other hand, Tyahla and McClellan reported fatigue test results of OH specimens of IM6/3100 and IM6/F650 CF/BMI composite materials with [0°(50%)/±45°(40%)/ 90°(10%)] layup for *R*=-1 and 10 (Tyahla & McClellan, 1988). Though IM6/3100 experienced longer lives during compression-only cycling (*R*=10) than reversed cycling (*R*=-1) on the basis of S_{max}-*N* diagrams under CTD and RTD conditions, IM6/F650 showed no extension of life during compression-only cycling compared to reversal cycling. They described that perhaps fatigue life in the case of IM6/F650 was controlled by delamination growth with compression loading and failure would occur when delaminations grew to a critical size.

The test results and discussion described above show that the repeated compression-load component of a tension-compression fatigue test has a large effect on fatigue strength over the entire life region, together with the maximum compression stress in the-short life region. The repeated tension-stress component has an effect only in the long-life region. This phenomenon is explained delamination growth in tension-compression fatigue being mainly driven by compression load repetition while final failure is generated by delamination buckling. This phenomenon and its interpretation are particularly noteworthy.

4.6 Comparison of fatigue data at room temperature obtained by the authors and Hirano

As stated in the introduction, Hirano reported *S-N* test results at RT for a G40-800/5260 CF/BMI composite material using a small number of specimens (Hirano, 2001). This section will compare his data with those obtained in the present study. He used OH specimens 38.1 mm wide, and with other dimensions such as the hole diameter, stacking sequence, and thickness the same as those in this study. The loading conditions of the fatigue tests were R=0.05 for tension fatigue, R=20 for compression fatigue, and R=-1 for tension-compression fatigue. The combination of R and the number of specimens tested, n, are {R=0.05, n=4(1)}, {R=20, n=3(1)}, and {R=-1, n=5}, where the figure in ( ) is the number of unbroken specimens. Since there are several differences between his and the authors' investigations, the sets of data are compared in the following way: (1) Net section stress is used. (2) Stress range is used, because R values are different in tension fatigue and compression fatigue tests. (3) Only Hirano's failure data are used. The results compared are as follows: (1) Both tension fatigue strength and compression fatigue strength in the present study are slightly higher than those given by Hirano; however, the difference is regarded as falling within the scatter band of data in the present study. (2) The tension-compression fatigue strength was equivalent in both investigations. Therefore, (3) it can be considered that the tension-compression fatigue strength was in agreement with the compression fatigue strength expressed by S_{range} as in the case of the present investigation. The results mentioned above are considered to indicate that the fatigue test results obtained by both investigations are effective and can be used as reference data. Moreover, the use of net section stress and stress range was effective in comparing the fatigue test results obtained for the different specimen width and R.

5. Conclusions

This study determined the static strength of NH (non-hole) and OH (open-hole) specimens and the fatigue strength of OH specimens made of a G40-800/5260 CF/BMI high-temperature polymer composite material with a quasi-isotropic layup at RT (room temperature) and high temperatures, mainly 150°C, where OH static and fatigue strengths were represented by net section stress. Major conclusions are as follows:

1. This study generated systematic test results of the static and fatigue strengths at RT and high temperatures and presented the original data in mathematical tables available for reference data.
2. NHT (non-hole tension) static strength, OHT (open-hole tension) static strength, and OHT fatigue strength (R=0.1) are classified as fiber-dominated properties; however, they have some weak matrix-dependence and are slightly influenced by temperature. Furthermore, due to its slight matrix dependence, OHT fatigue strength is weakly dependent on the number of load cycles.
3. NHC (non-hole compression) static strength, OHC (open-hole compression) static strength, OHC fatigue strength (R=10), and OHTC (open-hole tension-compression) fatigue strength (R=-1) are classified as matrix-dominated properties and are temperature-dependent. Because of the matrix dependence, OHC and OHTC fatigue strengths are fairly dependent on the number of load cycles.
4. The fiber fracture of 45° plies was also observed in the static tensile failure of an NH specimen, though the static tensile strength was considered to be a strongly fiber-

dominated property. In the static compressive failure of NH and OH specimens, the rhombus shaped fracture and partial shear failure were observed on the side face. These failure modes were regarded as indicative of matrix-dominated fracturing.

5. An open hole greatly reduced static strength and this effect was larger for compressive strength than for tensile strength. The strength reduction due to the hole either for tension load or compression load was smaller at 150°C than at RT.
6. The static strength ratio (=compressive strength/tensile strength) was fairly low for both NH and OH specimens, except for the comparatively high ratio for NH static strength at RT. The fatigue strength ratio (=OHC fatigue strength/OHT fatigue strength) was generally lower than the static strength ratio, and it decreased to 50% at both RT and 150°C.
7. The S_{range}-N line of compression fatigue (R=10) and the S_{max}-N line of tension-compression fatigue (R=-1) gradually intersected each other at either RT or 150°C. Especially at RT the two S-N lines broadly overlapped. This fact indicates that the compression stress range mostly controlled fatigue lives in tension-compression fatigue tests at RT and 150°C.
8. The use of net section stress and stress range was effective in comparing the fatigue test results obtained for the different specimen width and R.
9. The static and fatigue strengths showed relatively small reduction from RT to 150°C except for NHC static strength. This is due to the use of a BMI resin for the material tested and demonstrates its practical utility at 150°C. However, structural designers should be careful about strength reduction when a structure has open holes and encounters compression loads in a high temperature environment.

6. References

Adam, T.; Gathercole, N., Reiter, H. & Harris, B. (1994). Life prediction for fatigue of T800/5245 carbon-fiber composites: II. Variable-amplitude loading. *International Journal of Fatigue*, Vol. 16, pp. 533-547. ISSN: 01421123.

Brandecker, B. & Hilgert, R. (1988). A320 full scale structural testing for fatigue and damage tolerance certification of metallic and composite structure. ICAS-88-5.8.1, pp. 1244-1256.

Fawcett, A.; Trostle, J. & Ward, S. (1997). 777 empennage certification approach. *Proc. 11th International Conference on Composite Materials*, Gold Coast, pp. I-178/I-199.

Gathercole, N.; Reiter, H., Adam, T., & Harris, B. (1994). Life prediction for fatigue of T800/5245 Carbon-Fiber Composites: I. Constant-Amplitude Loading. *International Journal of Fatigue*, Vol. 16, pp. 523-532. ISSN: 01421123.

Hirano, K. (2001). Long-term durability performance for advanced high temperature polymer matrix composites. *Proc. 13th International Conference on Composite Materials*, ID-1299 (CD-ROM), Beijing.

JAXA (Japan Aerospace Exploration Agency). (2007). *Advanced Composites Database System*: JAXA-ACDB, Ver. 06-1. http://www.jaxa-acdb.com/.

Johnston, W.M. & Gates, T.S. (1998). The effects of stress and temperature on the open-hole tension fatigue behavior of a graphite/bismaleimide composite. *Composite Materials: Fatigue and Fracture*, ASTM STP 1330, pp. 179-198, American Society for Testing and Materials. ISSN: 0066-0558.

Marais, C.; Shimokawa, T. & Katoh, H. (2001). Compressive strength degradation relationship of carbon/BMI composites after thermal cycling and aging for the second generation SST structures. *Proc. 13th International Conference on Composite Materials*, ID-1024 (CD-ROM), Beijing.

McConnell, V.P. (2009). Resins for the hot zone, Part II: BMIs, CEs, benzoxazines and phthalonitriles. *High Performance Composites*, Sept. 2009. http://www.compositesworld.com/articles/resins-for-the-hot-zone-part-ii-bmis-ces-benzoxazines-and-phthalonitriles.

Nagao, Y.; Iwahori, Y., Hirano, Y. & Aoki, Y. (2007). Low cost composite wing structure manufacturing technology development program in JAXA, *Proc. 16th International Conference on Composite Materials*, Kyoto (CD-ROM).

Niu, M.C.Y. (1996). Composite Airframe Structures - *Practical Information and Data* -, Hong Kong Conmilit Press Ltd., p. 75. ISBN: 9627128066.

Pilato, L.A. & Michno, M.J. (1994). *Advanced Composite Materials*, Springer-Verlag, p. 129 & p. 151. ISBN/ISSN: 3540575634/0387575634.

Rosenfeld, M.S. & Gause, L.W. (1981). Compression fatigue behavior of graphite/epoxy in the presence of stress raisers. *Fatigue of Fibrous Composite Materials*, *ASTM STP 723*, American Society for Testing and Materials, pp. 174-196. ISSN: 0066-0558.

Shimokawa, T.; Hamaguchi, Y., Kakuta, Y., & Katoh, H. (1999-a). Effect of isothermal aging on ultimate strength of high temperature composite materials for SST structures. *Journal of Composite Materials*, Vol. 33, No. 12, pp. 1104-1118. ISSN 0021-9983.

Shimokawa, T.; Hamaguchi, Y. & Katoh, H. (1999-b). Effect of moisture absorption on hot/wet compressive strength of T800H/PMR-15 carbon polyimide. *Journal of Composite Materials*, Vol. 33, No. 18, pp. 1685-1698. ISSN 0021-9983.

Shimokawa, T.; Katoh, H., Hamaguchi, Y., Sanbongi, S., Mizuno, H., Nakamura, H., Asagumo, R., & Tamura, H. (2002). Effect of thermal cycling on microcracking and strength degradation of high-temperature polymer composite materials for use in next-generation SST structures. *Journal of Composite Materials*, Vol. 36, No. 7, pp. 85-895. ISSN 0021-9983.

Shimokawa, T.; Kakuta, Y., Saeki, D. & Kogo, Y. (2007). Carbon plain-weave fabric low-temperature vacuum cure epoxy composite: static and fatigue strength at room and high temperatures and practicality evaluation. *Journal of Composite Materials*, Vol. 41, No. 18, pp. 2245-2265. ISSN 0021-9983.

Shimokawa, T.; Kakuta, Y., Hamaguchi, Y. & Aiyama, T. (2008). Static and fatigue strengths of a G40-800/5260 carbon fiber/bismaleimide composite material at room temperature and 150°C. *Journal of Composite Materials*, Vol. 42, No. 7, pp. 655-679. ISSN 0021-9983.

Tyahla, S.T. & McClellan, P.S., Jr. (1988). Durability and damage tolerance of bismaleimide composites - Volume I: Technical Report. *AFWAL-TR-88-3026*, Wright-Patterson Air Force Base.

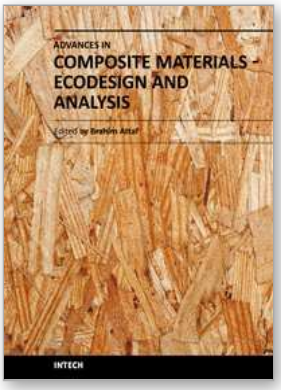

Advances in Composite Materials - Ecodesign and Analysis
Edited by Dr. Brahim Attaf

ISBN 978-953-307-150-3
Hard cover, 642 pages
Publisher InTech
Published online 16, March, 2011
Published in print edition March, 2011

By adopting the principles of sustainable design and cleaner production, this important book opens a new challenge in the world of composite materials and explores the achieved advancements of specialists in their respective areas of research and innovation. Contributions coming from both spaces of academia and industry were so diversified that the 28 chapters composing the book have been grouped into the following main parts: sustainable materials and ecodesign aspects, composite materials and curing processes, modelling and testing, strength of adhesive joints, characterization and thermal behaviour, all of which provides an invaluable overview of this fascinating subject area. Results achieved from theoretical, numerical and experimental investigations can help designers, manufacturers and suppliers involved with high-tech composite materials to boost competitiveness and innovation productivity.

InTech Europe
University Campus STeP Ri
Slavka Krautzeka 83/A
51000 Rijeka, Croatia
Phone: +385 (51) 770 447
Fax: +385 (51) 686 166
www.intechopen.com

InTech China
Unit 405, Office Block, Hotel Equatorial Shanghai
No.65, Yan An Road (West), Shanghai, 200040, China
中国上海市延安西路65号上海国际贵都大饭店办公楼405单元
Phone: +86-21-62489820
Fax: +86-21-62489821

The effects of reinforcement structures and hybrid types on the inter-laminar shear strength (ILSS) of carbon-glass hybrid fibers/bismaleimide composites under thermo-oxidative aging conditions were investigated. The process resulted in progressive deterioration of the matrix and fiber/matrix interfaces, in the form of chain scissions, weight loss, and fiber/matrix debonding, which significantly led to the decrease of the ILSS of composites. Moreover, the three-dimensional orthogonal woven hybrid composites (3D composites) showed higher ILSS retention rate than those of the laminated orthogona The composite system studied was a graphite fiber-reinforced bismaleimide thermoset, IM7/5260. The samples were subjected to both high and low temperature profiles as well as high-strain and low-strain profiles.Â W.H. Prosser, The Propagation Characteristics of the Plate Modes of Acoustic Emission Waves in Thin Aluminum Plates and Thin Graphite/Epoxy Composite Plates and Tubes, NASA Technical Memorandum 104187, Nov 1991Google Scholar. 21.Â W.M. Johnston and T.S. Gates, The Effects of Stress and Temperature on the Open-Hole Tension Fatigue Behavior of a Graphite/Bismaleimide Composite, Composite Materials: Fatigue and Fracture, Seventh Volume, STP 1330, R.B. Bucinell, Ed., ASTM, 1998, p 179â€“198Google Scholar. Copyright information. A material with a higher elastic modulus would likely show a lower degree of heating at a given stress, due to lower energy input. For the specimens monitored at 70 MPa, temperature increase appeared similar at both 21Â°C and 80Â°C and was significantly. 5.Â 1. Ivo Cerny, & Rayner M. Mayer, â€œEvaluation of Static and Fatigue Strength of Long Fiber GRP Composite Material Considering Moisture Effects,â€ Composite Structures, 92 (2010), pp. 2035-2038. 2. Toshiyuki Shimokawa, Yoshiaki Kakuta, Yasumasa Hamaguchi, & Takenori Aiyama, â€œStatic and Fatigue Strength of a G40-800/5260 Carbon Fiber/Bismaleimide Composite Material at Room Temperature and 150Â°C,â€ Journal of Composite Materials 42 (2008), pp. 655-679.